Saudi Pharmaceutical Journal 32 (2024) 101962

HOSTED BY

Contents lists available at ScienceDirect

Saudi Pharmaceutical Journal

journal homepage: www.sciencedirect.com

Original article

Synthesis of tetrazole hybridized with thiazole, thiophene or thiadiazole derivatives, molecular modelling and antimicrobial activity

Matokah M. Abualnaja [a], Adel I. Alalawy [b], Omar M. Alatawi [c], Ali H. Alessa [c], Ahmad Fawzi Qarah [d], Alaa M. Alqahtani [e], Majid A. Bamaga [f], Nashwa M. El-Metwaly [a,g,*]

[a] Department of Chemistry, Collage of Science, Umm Al-Qura University, Makkah 24230, Saudi Arabia
[b] Department of Biochemistry, Faculty of Science, University of Tabuk, Saudi Arabia
[c] Department of Chemistry, Faculty of Science, University of Tabuk, Tabuk 47512, Saudi Arabia
[d] Department of Chemistry, College of Science, Taibah University, Madinah, P.O. Box 344, Saudi Arabia
[e] Department of Pharmaceutical Sciences, Faculty of Pharmacy, Umm Al-Qura University, Makkah 21955, Saudi Arabia
[f] Department of Environment and Health Research, Umm Al-Qura University, Makkah, Saudi Arabia
[g] Department of Chemistry, Faculty of Science, Mansoura University, El-Gomhoria Street, 35516, Egypt

ARTICLE INFO

Keywords:
Tetrazole-thiophene hybrids
DNA Gyrase
DFT modelling
Docking
4URO

ABSTRACT

Background: Tetrazole-based derivatives and their electronic structures have displayed interesting antimicrobial activity.

Methods: The tetrazole-based hybrids linked with thiazole, thiophene and thiadiazole ring systems have been synthesized through various chemical reactions. The computational method DFT/B3LYP has been utilized to calculate their electronic properties. The antimicrobial effectiveness was investigated against representative bacterial and fungal strains. Additionally, the synthesized derivatives binding interaction was stimulated by docking program against PDB ID: 4URO as a model of the ATP binding domain of *S. aureus* DNA Gyrase subunit B.

Results: The structures of the synthesized tetrazole-based derivatives were confirmed by IR, NMR, and Mass spectroscopic data. The DFT/B3LYP method showed that the thiadiazole derivatives **9a–c** had lower $\Delta E_{H\text{-}L}$ than the thiophenes **7a–c** and thiazoles **5a–c**. The hybrids **5b**, **5c**, and **7b** exhibited proper antibacterial activity against Gram's +ve bacterial strains (*S. aureus* and *S. pneumonia*), while **9a** displayed potent activity towards Gram's -ve bacterial strains (*S. typhimurium* and *E. coli*). Meanwhile, derivatives **5a-b**, **7a**, **7c**, and **9c** showed good effectiveness towards fungal strain (*C. albicans*).

Conclusion: The study provides valuable tetrazole core-linked heterocyclic rings and opens the door to further research on their electrical characteristics and applications. Tetrazoles and thiazoles have antibacterial properties in pharmacological frameworks, making these hybrids potential lead molecules for drug development. The conclusion summarizes the data and suggests that the synthesized chemicals' interaction with a particular protein domain suggests focused biological activity.

1. Introduction

Because of their various biological and pharmacological effects, heterocyclic compounds have long piqued the curiosity of organic and medicinal chemists (Shukla et al., 2017, Liu et al., 2019, Mermer et al., 2019, Baranwal et al., 2023). The existence of several heteroatoms inside these cyclic structures imparts distinct reactivity and interaction patterns, making them appealing drug design targets (Peerzada et al., 2021, Wu and Meanwell, 2021). Among them, molecules having thiophene, thiazole, thiadiazole, and tetrazole rings have gotten a lot of interest because of their diverse biological effects; including antibacterial properties (Jain et al., 2013, Kotian et al., 2020, Arshad et al., 2022). Thiophene has a five-membered ring structure with four carbon atoms and one sulphur atom. The sulphur atom gives the ring an electron-rich

* Corresponding author at: Department of Chemistry, Collage of Science, Umm Al-Qura University, Makkah 24230, Saudi Arabia.
E-mail addresses: mmabualnaj@uqu.edu.sa (M.M. Abualnaja), aalalawy@ut.edu.sa (A.I. Alalawy), omalataw@ut.edu.sa (O.M. Alatawi), aalissaa@ut.edu.sa (A.H. Alessa), aqaraah@taibahu.edu.sa (A. Fawzi Qarah), amqahtan@uqu.edu.sa (A.M. Alqahtani), mabamag@uqu.edu.sa (M.A. Bamaga), nmmohamed@uqu.edu.sa (N.M. El-Metwaly).

https://doi.org/10.1016/j.jsps.2024.101962
Received 10 November 2023; Accepted 19 January 2024
Available online 20 January 2024

character, making it an important location for electrophilic assault and promoting interactions with biological targets (Gehringer and Laufer, 2019). Temporarily, the 1,3-thiazole ring has a sulphur atom next to a nitrogen atom in position three. The closeness of these two heteroatoms allows for a variety of electrical effects and interactions, making it a critical core for many physiologically active compounds (Petrou et al., 2021). Similarly, ring system refers to a five-membered ring having two nitrogen atoms and one sulphur atom. It might take the form of 1,2,3-thiadiazole or 1,3,4-thiadiazole depending on its replacement. Because it contains numerous nitrogen atoms as well as a sulphur atom, it is extremely reactive and suited for interactions with biological things (Serban et al., 2018). Meanwhile, tetrazole is a five-membered ring that contains four nitrogen atoms. Because of the high density of nitrogen atoms in the ring structure, tetrazoles are very electron-deficient and polar, allowing them to engage in diverse hydrogen bonding interactions in several biological medications (Fig. 1) (Cardoso-Ortiz et al., 2023). We discovered biological activity for various heterocyclic derivatives connected to the tetrazole ring, such as thiophene-tetrazole, thiazole-tetrazole, and thiadiazole-tetrazole analogues, in the previous survey. Thiophene rings with their sulphur atoms, on the other hand, can interact uniquely with biological targets inside the Thiophene-Tetrazole structure (Levin, 1997). There is potential for enhanced bioavailability and lower metabolic susceptibility when connected to the tetrazole moiety, which is an isostere of the carboxylic acid group (Bredael et al., 2022). Thiophene-tetrazole compounds have shown a variety of biological properties, including antibacterial activity. Likewise, thiazole-tetrazole derivatives have shown promising antimicrobial activities, likely due to their dual heterocyclic nature enhancing interactions with bacterial enzymes or proteins (Ahmadi et al., 2022). Similarly, thiadiazole-tetrazole analogues: thiadiazoles are recognised for their various biological actions because they contain both nitrogen and sulphur atoms. When coupled with the tetrazole ring, the resultant compounds frequently exhibit increased potency and activity spectrum. The coupling of thiadiazole and tetrazole moieties can produce compounds that disrupt biological processes, resulting in therapeutic drugs (Oballa et al., 2011). The combination of the aforementioned heterocycles, particularly when connected with tetrazole moieties, has demonstrated effectiveness against a variety of microorganisms (Preetham et al., 2022). Thiophene, thiazole, and thiadiazole's electron-rich character, along with the electron-deficient and polar nature of tetrazoles, may help in penetrating bacterial cell walls and disrupting critical bacterial enzymes or proteins (Liu et al., 2019). The electron-donating capacity of the sulphur and nitrogen atoms in thiophenes, thiazoles, and thiadiazoles can interact with important bacterial proteins, albeit the exact method varies depending on the unique structure of the chemical (Beno et al., 2015). The tetrazole moiety may enhance these interactions, allowing for the interruption of bacterial growth and function (Hoque et al., 2019). Our study aimed to synthesise new tetrazole derivatives hybridised with thiazole, thiophene, or thiadiazole derivatives and elucidate their corrected structures using various spectroscopic tools, as well as discover their antimicrobial activities and estimate them reactivates using theoretical studies such as molecular modelling and docking instigations.

2. Experimental

2.1. Instruments

Melting points were measured on a Gallenkamp electric apparatus. The IR spectral analyses (KBr discs) were recorded on a Thermo Scientific Nicolet iS10 FTIR spectrometer. The ^{1}H NMR (500 MHz) and the ^{13}C NMR spectra (125 MHz) were recorded in DMSO-d_6 using a JEOL spectrometer at those respective frequencies. Mass spectra were collected using a Quadrupole GC–MS (DSQII) instrument at 70 eV. Elemental analyses of C, H, and N were obtained using a Perkin Elmer 2400 analyzer.

2.2. Synthesis of 1-(4-acetylphenyl)-1H-tetrazole (2)

The title compound was prepared by reflux a mixture of 4-aminoacetophenone, sodium azide, and triethylorthoformate in acetic acid according the previously described methodology (Vembu et al., 2016).

2.3. Synthesis of 1-(4-(2-bromoacetyl)-phenyl)-1H-tetrazole (3)

Bromine (1.04 mL, 20 mmol) was added portion wise to a solution of 1-(4-acetylphenyl)-1*H*-tetrazole (**2**) (3.76 g, 20 mmol) in 30 mL dioxane-ether (1:2) with cooling at 0–5 °C and stirring over an hour. The reaction mixture was further stirred for 2 h with cooling. The reaction mixture was diluted with ether (90 mL) and water (90 mL). The ethereal layer was separated, washed with 1 M sodium bicarbonate aqueous solution, and dried over Na_2SO_4. The ether extract was distilled off to afford the targeting tetrazolyl-phenacyl bromide compound **3**.

Yield = 67 %, m.p. = 171–172 °C. IR (ν/cm^{-1}): 1688 (C═O), 1654 (C═N). ^{1}H NMR (δ/ppm): 4.34 (s, 2H, -COCH$_2$Br), 7.71 (d, J = 8.50 Hz, 2H), 7.83 (d, J = 8.50 Hz, 2H), 9.46 (s, 1H, tetrazole-H). ^{13}C NMR (δ/ppm): 31.64, 122.31 (2C), 128.55 (2C), 133.92, 138.40, 141.13, 190.47. Anal. Calcd. for $C_9H_7BrN_4O$ (266.00): C, 40.47; H, 2.64; N, 20.98 %. Found: C, 40.55; H, 2.61; N, 21.06 %.

2.4. Synthesis of 2-(2-arylidene-hydrazinyl)-4-(4-(1H-tetrazol-1-yl) phenyl)thiazoles 5a-c

1-(4-(2-Bromoacetyl)-phenyl)-1*H*-tetrazole (**3**) (1.06 g, 4 mmol) was added to a solution of each thiosemicarbazone compound **4a**, **4b** or **4c** (4 mmol) in ethanol (30 mL) and triethylamine (0.2 mL) were added. The solution was refluxed with stirring for 4 h and then allowed to cool. The solid was collected by filtration and crystallized from ethanol to

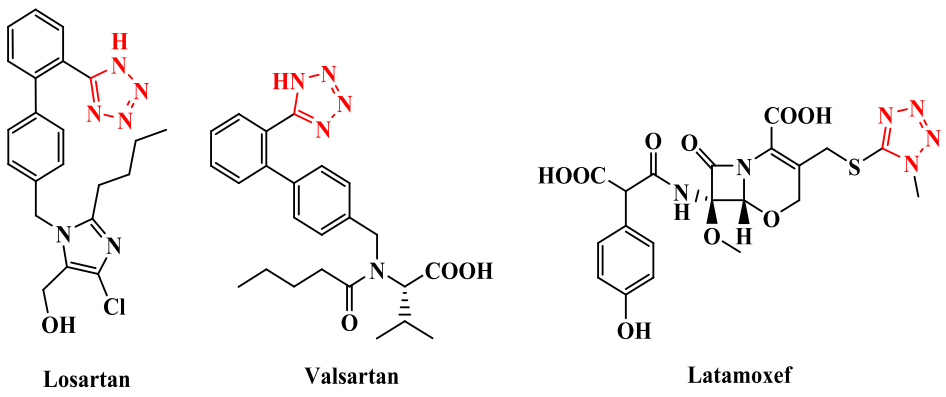

Fig. 1. Chemical structures of drug containing tetrazole-ring.

produce the targeting tetrazole-thiazole hybrids **5a**, **5b**, and **5c**, respectively.

4-(4-(1*H*-Tetrazol-1-yl)phenyl)-2-(2-(4-methylbenzylidene)hydrazinyl)thiazole (**5a**):

Yield = 63.5 %, m.p. = 233–234 °C. IR (ν/cm^{-1}): 3068 (C—H, sp^2), 1657 (C═N). ^{1}H NMR (δ/ppm): 2.34 (s, 3H, CH_3), 7.11 (s, 1H, thiazole-H), 7.36 (d, J = 8.50 Hz, 2H), 7.57 (d, J = 8.50 Hz, 2H), 7.74 (d, J = 8.50 Hz, 2H), 7.85 (d, J = 8.50 Hz, 2H), 7.94 (s, 1H, CH═N), 9.48 (s, 1H, tetrazole-H), 11.56 (s, 1H, N—H). ^{13}C NMR (δ/ppm): 21.24, 106.81, 125.77 (2C), 126.48 (2C), 127.89 (2C), 129.08 (2C), 131.13, 132.93, 133.37, 139.96, 141.18, 144.65, 147.57, 170.32. MS *m/z* (%): 361 (M$^+$, 26.34). Anal. Calcd. for $C_{18}H_{15}N_7S$ (361.11): C, 59.82; H, 4.18; N, 27.13 %. Found: C, 60.02; H, 4.12; N, 27.24 %.

4-(4-(1*H*-Tetrazol-1-yl)phenyl)-2-(2-(4-methoxybenzylidene)hydrazinyl)thiazole (**5b**):

Yield = 70.3 %, m.p. = 246–247 °C. IR (ν/cm^{-1}): 3077 (C—H, sp^2), 1652 (C═N). ^{1}H NMR (δ/ppm): 3.79 (s, 3H, OCH_3), 7.01 (d, J = 8.50 Hz, 2H), 7.09 (s, 1H, thiazole-H), 7.33 (d, J = 8.50 Hz, 2H), 7.76 (d, J = 8.50 Hz, 2H), 7.84 (d, J = 8.50 Hz, 2H), 7.91 (s, 1H, CH═N), 9.50 (s, 1H, tetrazole-H), 11.43 (s, 1H, N—H). ^{13}C NMR (δ/ppm): 55.87, 106.69, 114.41 (2C), 125.58 (2C), 126.52, 128.05 (2C), 129.64 (2C), 132.97, 133.40, 141.21, 144.80, 147.73, 161.33, 170.47. MS *m/z* (%): 377 (M$^+$, 33.81). Anal. Calcd. for $C_{18}H_{15}N_7OS$ (377.11): C, 57.28; H, 4.01; N, 25.98 %. Found: C, 57.13; H, 3.96; N, 25.90 %.

4-(4-(1*H*-Tetrazol-1-yl)phenyl)-2-(2-(4-chlorobenzylidene)hydrazinyl)thiazole (**5c**):

Yield = 65.8 %, m.p. = 220–221 °C. IR (ν/cm^{-1}): 3071 (C—H, sp^2), 1659 (C═N). ^{1}H NMR (δ/ppm): 7.05 (s, 1H, thiazole-H), 7.43 (d, J = 8.50 Hz, 2H), 7.61 (d, J = 8.50 Hz, 2H), 7.70 (d, J = 8.50 Hz, 2H), 7.79 (d, J = 8.50 Hz, 2H), 7.90 (s, 1H, CH═N), 9.49 (s, 1H, tetrazole-H), 11.62 (s, 1H, N—H). ^{13}C NMR (δ/ppm): 106.53, 125.67 (2C), 127.80 (2C), 129.11 (2C), 130.08 (2C), 132.88, 133.34, 134.36, 136.07, 141.17, 144.72, 147.64, 170.40. MS *m/z* (%): 383 (M$^+$, Cl-37, 6.35), 381 (M$^+$, Cl-35, 19.66). Anal. Calcd. for $C_{17}H_{12}ClN_7S$ (381.06): C, 53.47; H, 3.17; N, 25.68 %. Found: C, 53.30; H, 3.24; N, 25.79 %.

*2.5. Synthesis of 4-amino-3-substituted-5-(4-(1H-tetrazol-1-yl)benzoyl)-2-(phenylamino)-thiophenes **7a-c***

Each of the thiocarbamoyl compound **6a**, **6b**, or **6c** (3 mmol) was solubilized in 30 mL ethanol. Then, 1-(4-(2-Bromoacetyl)-phenyl)-1*H*-tetrazole (**3**) (0.80 g, 3 mmol) and 0.2 mL triethylamine were added. The mixture was refluxed for 4 h and then cooled to 25 °C in order to form a precipitate. Finally, the solid was crystallized from tetrahydrofuran to afford the conforming tetrazole-thiophene hybrids **7a**, **7b**, and **7c**, respectively.

4-Amino-3-cyano-5-(4-(1*H*-tetrazol-1-yl)benzoyl)-2-(phenylamino) thiophene (**7a**):

Yield = 76.5 %, m.p. = 269–270 °C. IR (ν/cm^{-1}): 3326, 3257, 3183 (–NH_2 and N—H), 2196 (C≡N), 1651 (C═N), 1604 (C═O). ^{1}H NMR (δ/ppm): 6.87 (s, 2H, –NH_2), 7.12–7.28 (m, 5H), 7.71 (d, J = 8.50 Hz, 2H), 7.79 (d, J = 8.50 Hz, 2H), 9.48 (s, 1H, tetrazole-H), 10.09 (s, 1H, N—H). ^{13}C NMR (δ/ppm): 84.08, 97.38, 115.28, 119.25 (2C), 121.13 (2C), 123.33, 128.87 (2C), 129.67 (2C), 136.92, 137.50, 139.41, 141.15, 158.54, 160.19, 186.44. MS *m/z* (%): 387 (M$^+$, 41.27). Anal. Calcd. for $C_{19}H_{13}N_7OS$ (387.09): C, 58.90; H, 3.38; N, 25.31 %. Found: C, 59.03; H, 3.35; N, 25.24 %.

Ethyl 5-(4-(1*H*-tetrazol-1-yl)benzoyl)-4-amino-2-(phenylamino) thiophene-3-carboxylate (**7b**):

Yield = 80.8 %, m.p. = 255–256 °C. IR (ν/cm^{-1}): 3311, 3251, 3176 (–NH_2 and N—H), 2191 (C≡N), 1655 (C═N), 1641 (C═O), 1598 (C═O). ^{1}H NMR (δ/ppm): 1.31 (t, J = 7.00 Hz, 3H, CH_3), 4.29 (q, J = 7.00 Hz, 2H, CH_2), 6.28 (s, 2H, –NH_2), 7.19–7.33 (m, 5H), 7.70 (d, J = 8.50 Hz, 2H), 7.81 (d, J = 8.50 Hz, 2H), 9.47 (s, 1H, tetrazole-H), 10.16 (s, 1H, N—H). ^{13}C NMR (δ/ppm): 14.30, 61.13, 100.77, 119.21 (2C), 121.28 (2C), 121.62, 123.28, 128.70 (2C), 129.56 (2C), 137.04, 137.53, 139.38, 141.16, 145.85, 160.96, 163.46, 186.51. MS *m/z* (%): 434 (M$^+$, 36.95). Anal. Calcd. for $C_{21}H_{18}N_6O_3S$ (434.12): C, 58.05; H, 4.18; N, 19.34 %. Found: C, 58.21; H, 4.26; N, 19.25 %.

5-(4-(1*H*-Tetrazol-1-yl)benzoyl)-4-amino-2-(phenylamino)thiophene-3-carboxamide (**7c**):

Yield = 73.5 %, m.p. = 288–289 °C. IR (ν/cm^{-1}): 3330, 3292, 3264, 3202 (–NH_2 and N—H), 2202 (C≡N), 1661 (C═O and C═N), 1608 (C═O). ^{1}H NMR (δ/ppm): 6.33 (s, 2H, –NH_2), 6.87 (s, 2H, –$CONH_2$), 7.09–7.27 (m, 5H), 7.69 (d, J = 8.50 Hz, 2H), 7.76 (d, J = 8.50 Hz, 2H), 9.48 (s, 1H, tetrazole-H), 10.11 (s, 1H, N—H). ^{13}C NMR (δ/ppm): 101.61, 104.92, 119.36 (2C), 121.20 (2C), 123.41, 128.81 (2C), 129.70 (2C), 136.05, 136.87, 137.45, 139.53, 141.18, 164.18, 166.29, 186.58. MS *m/z* (%): 405 (M$^+$, 28.44). Anal. Calcd. for $C_{19}H_{15}N_7O_2S$ (405.10): C, 56.29; H, 3.73; N, 24.18 %. Found: C, 56.17; H, 3.77; N, 24.25 %.

*2.6. Synthesis of 2-(4-(1H-tetrazol-1-yl)phenyl)-N-(4-chlorophenyl)-2-oxoacetohydrazonoyl bromide **(8)***

A solution of sodium nitrite (0.84 g in 10 mL water) was added dropwise into a suspension of 4-chloroaniline (1.52 g, 12 mmol) in conc. hydrochloric acid (3.60 mL) in a temperature range of 0–5 °C. The diazonium salt that obtained was added dropwise to a stirred solution of 1-(4-(2-bromoacetyl)-phenyl)-1*H*-tetrazole (**3**) (3.19 g, 12 mmol) in 40 mL pyridine at 0–5 °C. The stirring was continued for additional two hours. The solid was collected, and subsequently crystallized using ethanol to furnish the targeting hydrazonoyl bromide **8**.

Yield = 58.0 %, m.p. = 201–202 °C. IR (ν/cm^{-1}): 3213 (N—H), 1667 (C═O), 1648 (C═N). ^{1}H NMR (δ/ppm): 7.11 (d, J = 8.50 Hz, 2H), 7.23 (d, J = 8.50 Hz, 2H), 7.73 (d, J = 8.50 Hz, 2H), 7.80 (d, J = 8.50 Hz, 2H), 9.48 (s, 1H, tetrazole-H), 12.66 (s, 1H, N—H). ^{13}C NMR (δ/ppm): 117.06 (2C), 121.94 (2C), 127.90, 129.27 (2C), 130.11 (2C), 136.25, 138.77, 141.15, 141.83, 147.58, 187.43. MS *m/z* (%): 406 (M$^+$, Br-81, 21.30), 404 (M$^+$, Br-79, 19.74). Anal. Calcd. for $C_{15}H_{10}BrClN_6O$ (404.00): C, 44.41; H, 2.48; N, 20.72 %. Found: C, 44.65; H, 2.58; N, 20.57 %.

*2.7. Synthesis of 2-substituted-5-(4-(1H-tetrazol-1-yl)benzoyl)-3-(4-chlorophenyl)-1,3,4-thiadiazoles **9a-c***

In a 100 mL RB-flask, a suspension of each thiocarbamoyl compound **6a**, **6b**, or **6c** (3 mmol) was and the hydrazonoyl bromide compound **8** (1.21 g, 3 mmol) in was refluxed for 4 h in dioxane (25 mL) and triethylamine (0.2 mL). The solid that formed after standing overnight was collected to furnish the conforming tetrazole-thiadiazole hybrids **9a**, **9b**, and **9c**, respectively.

2-(5-(4-(1*H*-Tetrazol-1-yl)benzoyl)-3-(4-chlorophenyl)-1,3,4-thiadiazol-2(3*H*)-ylidene)malononitrile (**9a**):

Yield = 61.5 %, m.p. = 277–278 °C. IR (ν/cm^{-1}): 2213 (C≡N), 1671 (C═O), 1651 (C═N). ^{1}H NMR (δ/ppm): 7.39 (d, J = 8.50 Hz, 2H), 7.57 (d, J = 8.50 Hz, 2H), 7.76 (d, J = 8.50 Hz, 2H), 7.83 (d, J = 8.50 Hz, 2H), 9.46 (s, 1H, tetrazole-H). ^{13}C NMR (δ/ppm): 68.50, 116.07 (2C), 122.01 (2C), 122.95 (2C), 128.64, 129.22 (2C), 129.87 (2C), 135.49, 138.36, 141.18, 142.17, 151.93, 169.76, 189.67. MS *m/z* (%): 434 (M$^+$, Cl-37, 15.88), 432 (M$^+$, Cl-35, 53.16). Anal. Calcd. for $C_{19}H_9ClN_8OS$ (432.03): C, 52.72; H, 2.10; N, 25.89 %. Found: C, 52.61; H, 2.05; N, 25.96 %.

Ethyl 2-(5-(4-(1*H*-tetrazol-1-yl)benzoyl)-3-(4-chlorophenyl)-1,3,4-thiadiazol-2(3*H*)-ylidene)-2-cyanoacetate (**9b**):

Yield = 58.7 %, m.p. = 262–263 °C. IR (ν/cm^{-1}): 2208 (C≡N), 1703 (C═O), 1682 (C═O), 1654 (C═N). ^{1}H NMR (δ/ppm): 1.32 (t, J = 7.00 Hz, 3H, CH_3), 4.28 (q, J = 7.00 Hz, 2H, CH_2), 7.40 (d, J = 8.50 Hz, 2H), 7.58 (d, J = 8.50 Hz, 2H), 7.75 (d, J = 8.50 Hz, 2H), 7.85 (d, J = 8.50 Hz, 2H), 9.47 (s, 1H, tetrazole-H). ^{13}C NMR (δ/ppm): 14.29, 61.10, 101.46, 116.63, 122.08 (2C), 122.88 (2C), 128.79, 129.17 (2C), 129.90 (2C), 135.56, 138.27, 141.21, 141.98, 152.29, 163.50, 166.02, 189.58. MS *m/z* (%): 481 (M$^+$, Cl-37, 12.39), 479 (M$^+$, Cl-35, 44.65). Anal. Calcd. for $C_{21}H_{14}ClN_7O_3S$ (479.06): C, 52.56; H, 2.94; N, 20.43 %. Found: C,

52.42; H, 3.01; N, 20.52 %.

2-(5-(4-(1*H*-Tetrazol-1-yl)benzoyl)-3-(4-chlorophenyl)-1,3,4-thiadiazol-2(3*H*)-ylidene)-2-cyanoacetamide (**9c**):

Yield = 64.8 %, m.p. = 301–302 °C. IR (ν/cm^{-1}): 3278, 3235 (–NH_2), 2211 (C≡N), broad at 1678 (2C═O), 1656 (C═N). ^{1}H NMR (δ/ppm): 7.14 (s, 2H, –NH_2), 7.38 (d, J = 8.50 Hz, 2H), 7.56 (d, J = 8.50 Hz, 2H), 7.70 (d, J = 8.50 Hz, 2H), 7.81 (d, J = 8.50 Hz, 2H), 9.48 (s, 1H, tetrazole-H). MS m/z (%): 452 (M^+, Cl-37, 5.91), 450 (M^+, Cl-35, 18.24). Anal. Calcd. for $C_{19}H_{11}ClN_8O_2S$ (450.04): C, 50.62; H, 2.46; N, 24.85 %. Found: C, 50.78; H, 2.53; N, 24.97 %.

2.8. DFT modelling

The studied derivatives were geometrically optimized by applying the B3LYP/6–311^{++}G(d,p) methodology in Gaussian 09 W program (Lee et al., 1988, Perdew and Wang, 1992, Becke, 1993, Frisch et al., 2009). GaussView software (Dennington et al., 2009) was employed to explore the resulting electronic properties and frontier molecular orbitals. The Fukui indices calculations (Delley, 2006) were carried out via B3LYP/DNP-3.5 incorporated in Materials Studio DMol3 module (BIOVIA 2017).

2.9. Antimicrobial assessment

The XTT assay was used to evaluate the antimicrobial efficacy of the synthesized tetrazole hybridized with thiazole, thiophene or thiadiazole derivatives have been inspected towards disparate pathogens like (two +ve Gram) bacteria, *Staphylococcus aureus* (*S. aureus*) and *Streptococcus pneumoniae* (*S. pneumoniae*), (two −ve Gram) bacteria, *Salmonella typhimurium* (*S.typhimurium*), and *Escherichia coli* (*E. coli*), as well fungi (*Candida albicans* and *Aspergillus fumigatus*). The antimicrobial methodology was employed over Calorimetric broth micro-dilution technique using reduction analyse was operated to determine the minimum inhibitory concentration (MIC), using Ciprofloxacin (antibacterial) and Miconazole (antifungal) as drug references as shown in supporting information file (Tunney et al., 2004, Fathallah et al., 2019, Omar et al., 2020).

2.10. Molecular docking

Accordingly, Type II topoisomerases rupture and link two DNA threads concurrently in an ATP-dependent mode. The ATP connecting site on DNA gyrase subunit B is an appealing target for the development of new antibacterial agents. PDB ID: 4URO from the RCSB library was employed to express the crystal configuration of the ATP interacting domain of *S. aureus* DNA Gyrase subunit B (Roszkowski et al., 2021). In the *in-silico* investigation of the antibacterial effectiveness of tetrazole hybridized with thiazole, thiophene or thiadiazole derivatives towards *S. aureus* DNA Gyrase subunit B.

3. Results

3.1. Synthesis of tetrazole hybridized with thiazole, thiophene or thiadiazole analogues

The tetrazole-thiazole hybrids **5a-c** presented in this research article were prepared in three synthetic steps as described in Scheme 1. In the first step, 4-aminoacetophenone and sodium azide was refluxed with triethylorthoformate in acidic medium in the light of the reported procedure to produce the precursor compound, 1-(4-acetylphenyl)-1*H*-tetrazole (**2**) (Vembu et al., 2016). The second step involves further treatment of compound **2** with bromine (Br_2) was carried out in mixed solvent of dioxane-ether (1:2) at 0–5 °C to afford the corresponding α-bromoketone, 1-(4-(2-bromoacetyl)-phenyl)-1*H*-tetrazole in 67 % yield. Finally, the key of this study, tetrazolyl phenacyl bromide compound **3** undergoes cyclization upon treatment with various

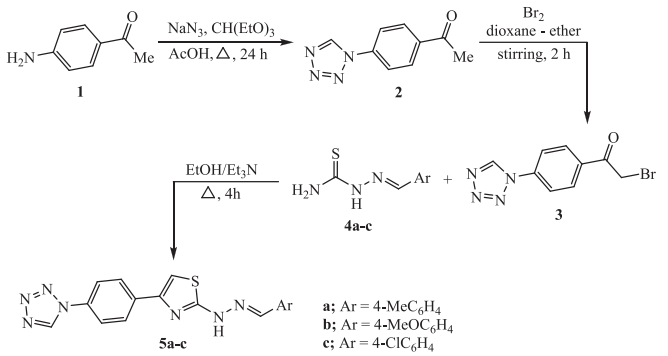

Scheme 1. Synthesis of tetrazole-thiazole hybrids **5a-c**.

thiosemicarbazone compounds **4a-c** (Hantzsch type reaction) to furnish the targeting tetrazole-thiazole hybrids **5a-c**. The reaction proceeds by refluxing the reaction components in ethanol and triethylamine for 4 h to obtain the tetrazole-thiazole hybrids **5a, 5b**, and **5c** in 63.5 %, 70.3 %, 65.8 % yields, respectively.

The reaction of 1-(4-(2-bromoacetyl)-phenyl)-1*H*-tetrazole with various thiocarbamoyl compounds **6a-c** substituted nitrile function was carried out in boiling ethanol and triethylamine. The resulting compounds were designated as the respective tetrazole-thiophene hybrids **7a**, **7b**, and **7c**, as shown in Scheme 2. The proposed mechanism entails the displacement of the bromine atom from the tetrazolyl phenacyl bromide compound **3** through nucleophilic substitution by sulfur in thiocarbamoyl compound **6**, resulting in the formation of the non-isolable sulfide intermediate (**A**). Subsequently, the methylene group underwent intramolecular addition to the nitrile function, leading to the formation of a thiophene ring and yielding the corresponding tetrazole-thiophene hybrids **7a-c**.

The reactivity of methylene group in the key 1-(4-(2-bromoacetyl)-phenyl)-1*H*-tetrazole facilitated the diazocoupling reaction with the diazonium salt obtained from 4-chloroaniline. The reaction proceeds by stirring in cold pyridine to furnish the corresponding hydrazonoyl bromide, 2-(4-(1*H*-tetrazol-1-yl)phenyl)-*N*-(4-chlorophenyl)-2-oxoacetohydrazonoyl bromide (**8**) (Scheme 3). The IR, ^{1}H NMR, ^{13}C NMR, and mass analyses were used to establish the structure of hydrazonoyl bromide compound **8**. In an alternative route, the reaction of each thiocarbamoyl compound **6a**, **6b**, or **6c** with hydrazonoyl bromide **8** proceeded in boiling dioxane and triethylamine to furnish a single product in each case. The structures of the isolated products were secured based on the spectroscopic data (IR, ^{1}H NMR, ^{13}C NMR, and mass analysis) and identified as the corresponding tetrazole-thiadiazole hybrids **9a**, **9b**, and **9c**. The proposed mechanism for the formation of the thiadiazole ring in the produced hybrids **9a-c** is described in the sequence depicted in Scheme 3. The reaction was initiated by a nucleophilic substitution of the bromine atom in hydrazonoyl bromide **8** to represent the non-isolable intermediate (**B**). Subsequently, the nucleophilic addition of N—H to the beta-carbon of the unsaturated nitrile moiety promoted the formation of intermediate (**C**), which underwent elimination of an aniline molecule (Gomha et al., 2017), leading to the production of the final product, tetrazole-thiadiazole ketones **9a-c**.

3.2. Molecular modelling

The geometrical optimization computations of **5a-c** compounds indicated that both **5a** and **5c** have perfect planar structures, while, compound **5b** has a non-planar configuration (Fig. 2 and Figure S1). Otherwise, the hybrids **7a-c** data revealed that only **7a** was planar while both of **7b** and **7c** have non-planar structures. As well, the **9a-c** compounds presented planar configurations except for **9b** (Fig. 2 and Figure S1).

The synthesized derivatives have analogous structure of HOMO that

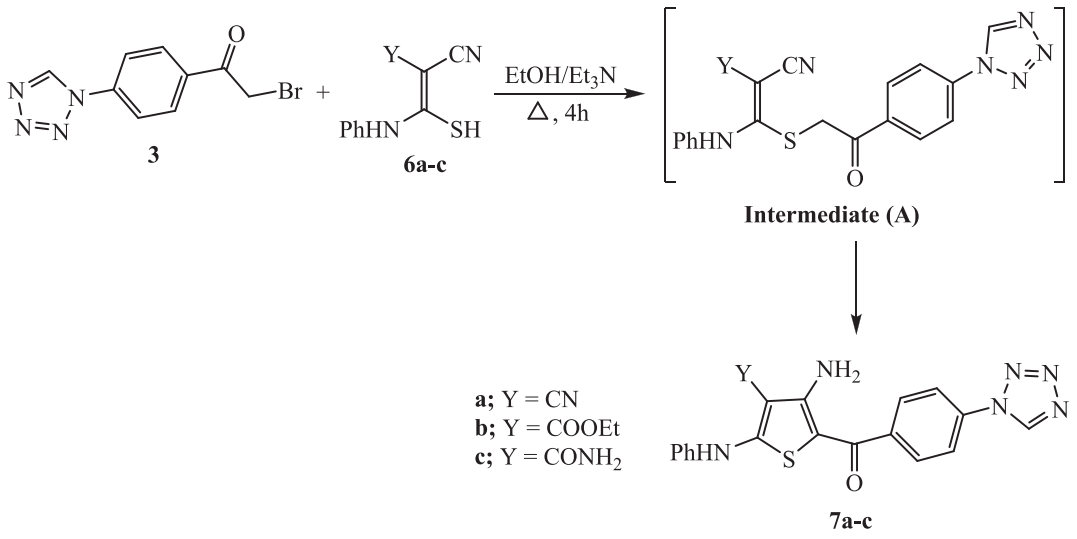

Scheme 2. Synthesis of tetrazole-thiophene hybrids **7a-c**.

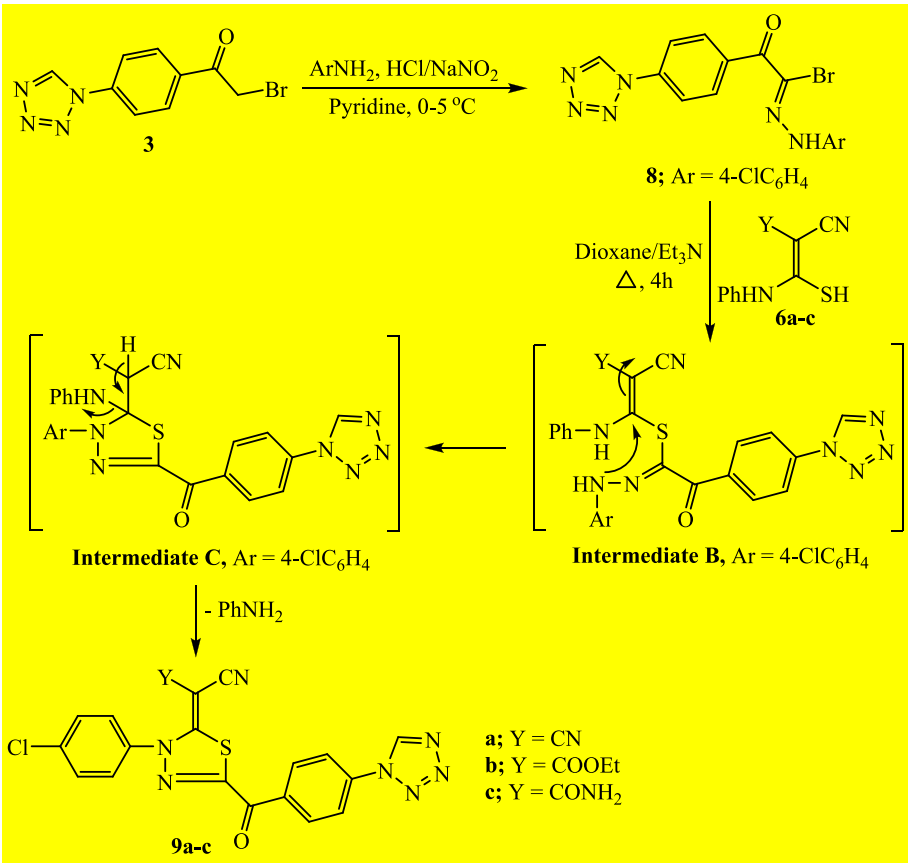

Scheme 3. Synthesis of tetrazole-thiadiazole hybrids **9a-c**.

built of the π-orbital of the entire molecule with minor participation of the tetrazole ring, although, their LUMO was constructed of the π*-orbital of the whole molecule (Fig. 3 & Figure S2). So, all the hybrids exhibited small energy gap ($\Delta E_{H\text{-}L}$), 1.64–2.51 eV (Table 1).

Besides, the chemical reactivity parameters, i.e., electronegativity (χ), global hardness (η), softness (δ), electrophilicity (ω), electron-donating power (ω^-) and electron-accepting power (ω^+) were determined *via* the E_H and E_L merits as follows (Xavier et al., 2015).

$$\chi = -\frac{1}{2}(E_{HOMO} + E_{LUMO})\eta = -\frac{1}{2}(E_{HOMO} - E_{LUMO})\delta = \frac{1}{\eta}\omega = \frac{\chi^2}{8\eta}\omega^- = \frac{(3I + A)^2}{16(I - A)}\omega^+ = \frac{(I + 3A)^2}{16(I - A)}$$

Additionally, the Mulliken's atomic charges in addition to the Fukui's indices were computed to explore the liable positions toward nucleophilic (f_k^+) and electrophilic (f_k^-) attacks (El Adnani et al., 2013, Mi et al., 2015, Olasunkanmi et al., 2016, Messali et al., 2018). But,

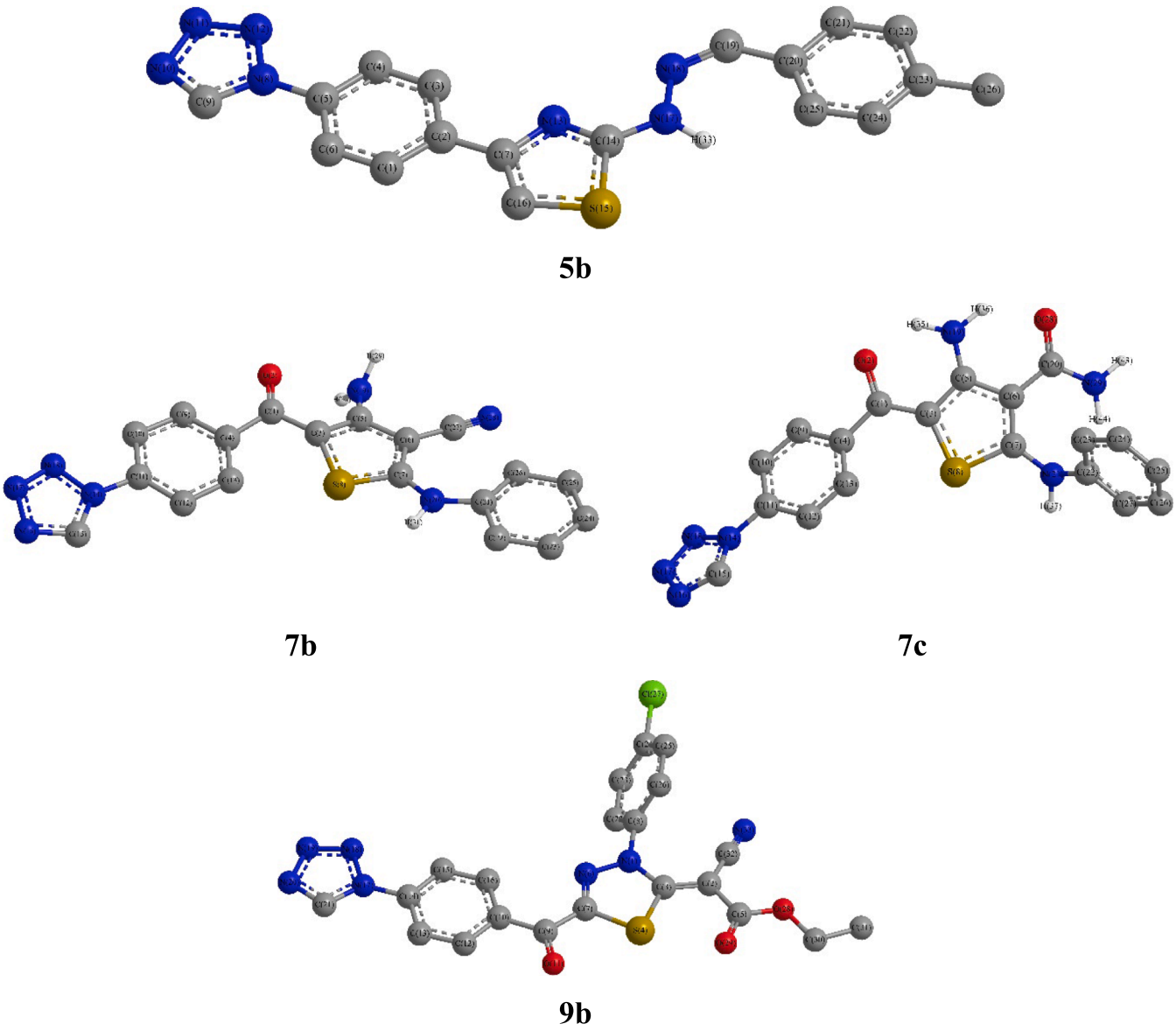

Fig. 2. Compounds **5b**, **7b-c** and **9b** DFT Optimized structures.

Fukui's indices occasionally became imprecise in estimating the vigorous locations, thus, the local relative electrophilicity (s_k^-/s_k^+) and nucleophilicity (s_k^+/s_k^-) factors were determined and matched with the consistent Fukui's indices (Roy et al., 1998a, Roy et al., 1998b, Roy et al., 1999).

the molecular polarizability (α_{total}), hyperpolarizabilities (β_{total}), and dipole moment (μ), of the studied hybrids were determined (Sun et al., 2003, Abraham et al., 2008, Karamanis et al., 2008) to explore more the molecule's softness and electron density distribution that basically impact the intermolecular interactions (Aziz et al., 2022), as well as, optical nonlinearity and response (Williams, 1984, Prasad and Williams, 1991, Shi, 2001, Khan et al., 2021) (Table 2).

$$\mu = (\mu_x^2 + \mu_y^2 + \mu_z^2)\alpha_{total} = \frac{(\alpha_{xx} + \alpha_{yy} + \alpha_{zz})}{3}$$

$$\beta_{total} = \sqrt{(\beta_{xxx} + \beta_{xyy} + \beta_{xzz})^2 + (\beta_{yyy} + \beta_{yzz} + \beta_{yxx})^2 + (\beta_{zzz} + \beta_{zxx} + \beta_{zyy})^2}$$

3.3. Antimicrobial evaluation

The results of the antimicrobial activity of the synthesized tetrazole hybridized with thiazole, thiophene, or thiadiazole derivatives **5a-c**, **7a-c**, and **9a-c** have been recorded in Table S6 (Fig. 4). In accordance with disparate pathogens like (two +ve Gram) bacteria, *Staphylococcus aureus* (*S. aureus*) and *Streptococcus pneumoniae* (*S. pneumoniae*), (two −ve Gram) bacteria, *Salmonella typhimurium* (*S. typhimurium*), and *Escherichia coli* (*E. coli*), as well fungi (*Candida albicans* and *Aspergillus fumigatus*) the prepared analogues were examined through XTT analyze.

3.4. Molecular docking

Molecular docking simulations were performed to assess the binding affinities and interaction profiles of different ligands with specific PDB: 4URO's amino-acids. The data is comprehensively compiled in the table S7, highlighting the binding energies (s), root mean square deviation (RMSD), nature of interactions, and the distance of interactions. The binding energies (s) ranged from −6.3135 kcal/mol to −8.3985 kcal/mol, with the ligand 'Novo' showing the strongest binding affinity (-8.3985 kcal/mol). Generally, more negative binding energies suggest

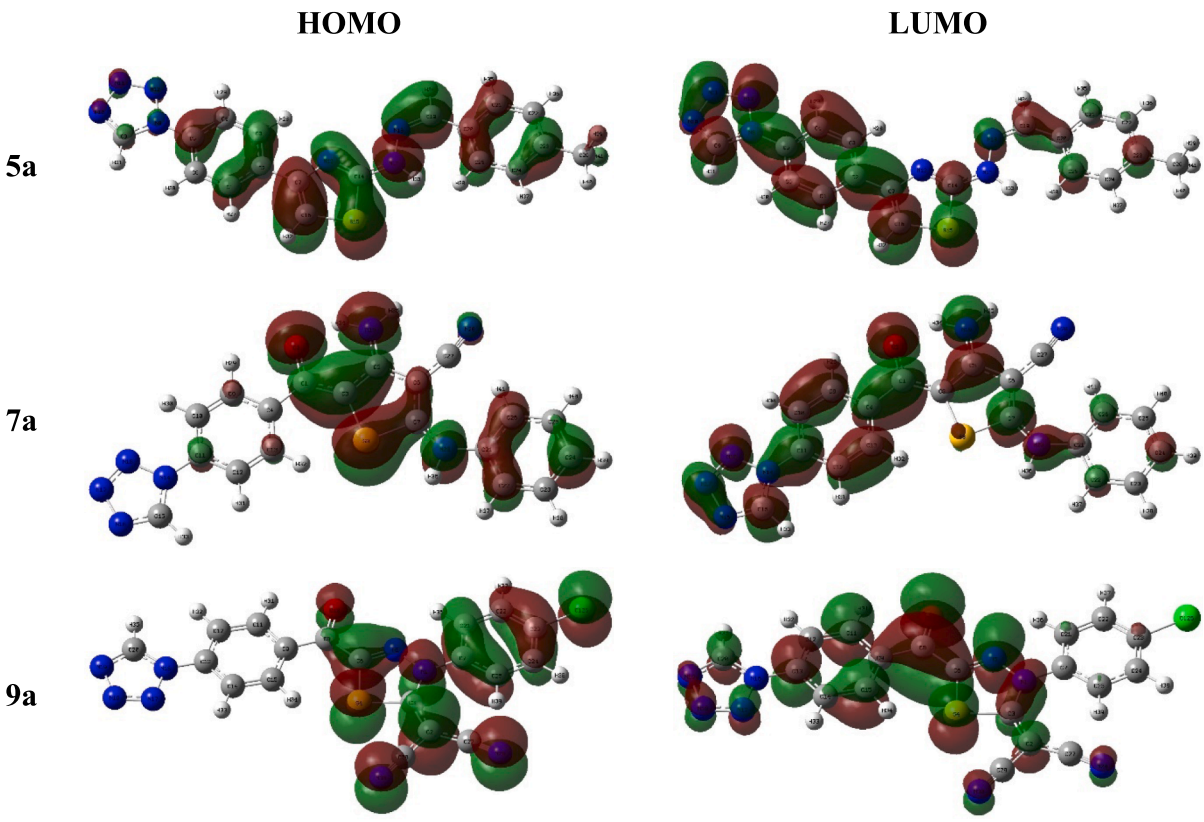

Fig. 3. The frontier molecular orbital of the synthesized compounds **5a**, **7a** and **9a**.

Table 1
FMO's energies and reactivity descriptors of studied compounds (eV).

Compound	E_H	E_L	ΔE_{H-L}	χ	η	δ	ω	ω+	ω-
5a	−5.95	−3.44	2.51	4.70	1.25	0.80	8.79	6.60	11.30
5b	−5.86	−3.35	2.51	4.61	1.26	0.80	8.45	6.31	10.91
5c	−6.16	−3.65	2.51	4.90	1.25	0.80	9.60	7.30	12.21
7a	−6.19	−4.05	2.14	5.12	1.07	0.93	12.21	9.79	14.91
7b	−5.91	−3.68	2.23	4.80	1.12	0.90	10.30	8.04	12.84
7c	−6.06	−3.90	2.16	4.98	1.08	0.93	11.47	9.11	14.09
9a	−7.03	−5.39	1.64	6.21	0.82	1.22	23.52	20.52	26.72
9b	−6.77	−5.02	1.75	5.89	0.88	1.14	19.82	16.98	22.87
9c	−6.79	−4.97	1.83	5.88	0.91	1.10	18.95	16.13	22.01

Table 2
The calculated dipole moment (μ), polarizability (α_{total}), polarizability anisotropy (Δα) and first-order hyperpolarizability (β_{total}) of investigated compounds.

Compound	μ (Debye)	μ/μ_{urea}	α_{total} (esu × 10^{-23})	Δα (esu × 10^{-23})	β_{total} (esu × 10^{-30})	$\beta_{total}/\beta_{urea}$
5a	12.16	8.85	2.43	1.14	9.97	26.67
5b	12.92	9.41	2.58	1.01	10.90	29.17
5c	9.24	6.73	2.73	1.37	7.05	18.85
7a	9.95	7.25	2.85	1.14	7.74	20.70
7b	13.01	9.47	3.00	0.6.1	10.30	27.59
7c	11.88	8.65	2.87	0.93	8.91	23.82
9a	6.99	5.09	3.22	0.73	5.39	14.43
9b	4.27	3.11	3.28	0.58	7.32	19.57
9c	2.18	1.58	3.17	1.18	4.54	12.14

stronger and more encouraging interactions. On the contrary, RMSD values give insight into the deviation of the docked pose from a reference pose, with smaller RMSD values indicating a closer alignment.

4. Discussions

4.1. Chemical structure elucidation of the synthesized hybrids

The structures of the isolated hybrids **5a-c** were elucidated by their compatible spectral analyses (IR, ^{1}H NMR, ^{13}C NMR, and MS). The ^{1}H NMR spectrum of tetrazole-thiazole hybrid **5a** (as an example) exhibited singlet at δ 2.34 and 7.11 ppm corresponding to the protons of a methyl group and thiazole-C5, respectively. The aromatic protons were assigned as four doublet signals in the region from δ 7.36 to 7.85 ppm. The proton of azomethine group (–CH═N-) was detected at δ 7.94 ppm. The protons of tetrazole-C5 and imino group (N—H) were recorded as singlet signals at δ 9.48 and 11.56 ppm, respectively. The molecular ion peak of **5a** was recorded at $m/z = 361$ with a relative intensity of 26.34 %, consistent with the formula $C_{18}H_{15}N_5S$.

Meanwhile, the three isolated hybrids **7a-c** provide satisfactory spectral analyses consistent with their designated structures. The IR spectrum of tetrazole-thiophene hybrid **7a** exhibited the absorptions of $–NH_2$ and N—H functions at 3326, 3257, and 3183 cm^{-1}. The nitrile and carbonyl groups were observed at their expected frequencies of 2196

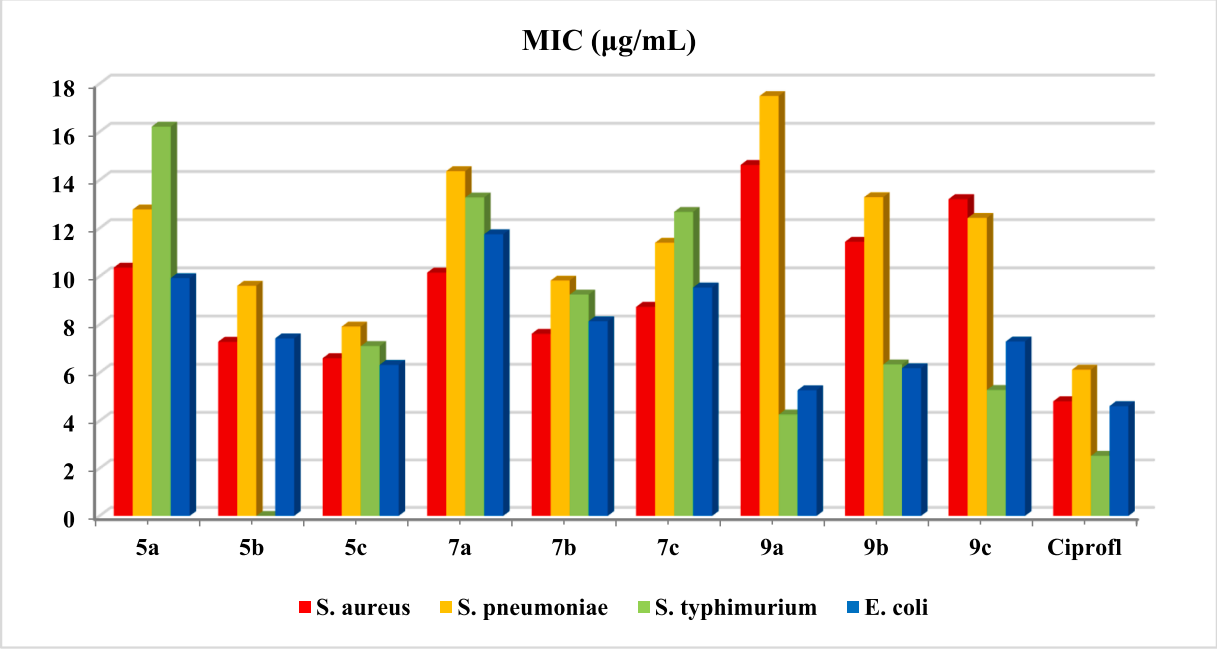

Fig. 4. MIC of the prepared tetrazole-analogues *via* XTT assay.

and 1604 cm^{-1}, respectively. The observed absorptions of the carbonyl-ketone function within the hybrids **7a-c** were determined at lower wavenumbers ranging from 1608 to 1598 cm^{-1}. This phenomenon can be explained due to the presence of extensive conjugation between the thiophene and benzene rings and the possible formation of intra-molecular H-bond between C═O and $–NH_2$ groups. The ^1H NMR spectrum of **7a** indicated the presence of amino group by the singlet at δ 6.87 ppm. The aromatic protons were observed as multiplet and doublet signals in the region from δ 7.12 to 7.79 ppm. The protons of tetrazole-C5 and N—H groups were assigned as singlet signals at δ 9.48 and 10.09 ppm.

4.2. Molecular modelling

The dihedral angles of **5b** showed that tetrazolyl ring was tilted on the adjacent phenyl by ~ 24.0°, $C^3_{(Phtetz)}$-$C^4_{(Phtetz)}$-$N^1_{(tetz)}$-$C^5_{(tetz)}$ = 156.4°, whereas, the hydrazo nitrogens were located above the thiazole's plane, e.g., $N^3_{(thz)}$–$C^2_{(thz)}$–$NH_{(Hz)}$-$N_{(Hz)}$ = −10.4°. Also, the methoxy benzylidene moiety was slanted on hydrazo nitrogen's by ~ 35°, i.e., $N_{(Hz)}$–$CH_{(El\ Adnani\ et\ al.,)}$-$C^1_{(PhBenz)}$- $C^2_{(PhBenz)}$ = 144.8° (Table S1). Alternatively, in the non-planar hybrids **7b-c** dihedral, the tetrazolyl ring was tilted on the phenyl's level, e.g., $C^3_{(Phtetz)}$-$C^4_{(Phtetz)}$-$N^1_{(tetz)}$-$C^5_{(tetz)}$ = 155.8° and 157.8°, respectively. Furthermore, their phenyl was tilted on the thiophene's plane as the $C^5_{(thp)}$–CO-$C^1_{(Phtetz)}$–$C^2_{(Phtetz)}$ = 27.9° and 28.6°, as well as, the phenylamine substituent was shifted out the thiophene, e.g., $NH_{(Hsiao\ et\ al.,)}$–$C^2_{(thp)}$-$S^1_{(thp)}$-$C^5_{(thp)}$ = −178.1° and −177.2° and $S^1_{(thp)}$–$C^2_{(thp)}$–$NH_{(Hsiao\ et\ al.,)}$-$C^1_{(Hsiao\ et\ al.,)}$ = −3.5° and −117.7°, respectively. The carboxylate in **7b** and carboxamide in **7c** displayed further deviation from planarity. As well, the non-planar **9b** data showed that the phenyl tetrazole and carbonyl moieties was slightly tilted on the thiadiazole's plane, i.e., $N^3_{(thdz)}$-$N^4_{(thdz)}$-$C^5_{(thdz)}$–CO = 178.0° and $C^5_{(thdz)}$–CO-$C^1_{(Phtetz)}$–$C^2_{(Phtetz)}$ = 177.5°, respectively. While, the thiadiazole substituents, chlorophenyl and cyanoacetate groups, exhibited strong for the former and weak deviation from planarity with thiadiazole ring, e.g., $C^2_{(thdz)}$–$N^3_{(thdz)}$-$C^1_{(Phthdz)}$-$C^1_{(Phthdz)}$ = 123.2° and $C_{(CNAc)}$–$C^2_{(thdz)}$-$S^1_{(thdz)}$-$C^5_{(thdz)}$ = −173.4°, respectively (Fig. 2 and Figure S1) (Table S1). Furthermore, a comparison was made between the DFT calculated bond's length in addition to angle and those found in x-ray of alike crystalline hybrids (Marsh, 2004, Studzińska et al., 2015), presented fair agreement where lengths were lengthy by maximal 0.26 Å (RMSD = 0.05–0.12) and angles divergences attaining 21.9° (RMSD = 4.2–8.9). These dissimilarities may be ascribed to that in solid crystal lattice, there are columbic interactions between molecules which absent in the quantum calculations conducted on a single gaseous molecule (Sajan et al., 2011) (Tables S2-S3).

The HOMO-LUMO energies strongly effect on the compound's chemical or biological behavior, where the molecule's aptitude to furnish or grab electrons determined by their values (Bulat et al., 2004) whereas bioactivity was greatly manipulated by their energy gap (Xavier et al., 2015, Bouchoucha et al., 2018, Makhlouf et al., 2018). The **5a-c** have analogous structure of HOMO that built of the π-orbital of the entire molecule with minor participation of the tetrazole ring, although, their LUMO was constructed of the π*-orbital of the whole molecule. Accordingly, they presented close values of HOMO and LUMO energies (E_H and E_H), −6.16 - −5.86 and −3.65 - −3.34 eV, respectively. Likewise, the derivatives **7a-c** possessed similar structure of HOMO and LUMO where the former consisted of π-orbital of the whole molecule except the phenyl tetrazole fragment whereas the latter was formed of the entire molecule's π*-orbital, and so, they displayed neighboring energies values. As well, the **9a-c** hybrids showed that the phenyl tetrazole did not involve in formation of HOMO, E_H = −7.03 - −6.77 eV, while the chlorophenyl group did not in LUMO, E_H = −5.39 - −4.97 eV (Fig. 3 & Figure S2) (Table 1). The aforementioned foundations designated that the thiadiazoles **9a-c** exhibited the lower HOMO-LUMO energies than thiophenes **7a-c** and thiazoles **5a-c**, respectively. Consequently, all the hybrids under examination displayed little energy gap ($\Delta E_{H\text{-}L}$), 1.64–2.51 eV, but the hybrids **9a-c** have the lowest while **5a-c** presented the highest values and may be arranged as **9a** < **9b** < **9c** < **7a** < **7c** < **7b** < **5a** = **5b** = **5c**.

As demonstrated in table 1, the **9a** hybrid possessed the greatest electronegativity (χ) and softness (δ), 6.21 and 1.22 eV, whereas **5b** was the least, 4.61 and 0.80 eV, respectively. While the hardness (η) data displayed reversed order where **9a** has the lowest value and **5b** has the highest and so **5b** may be the utmost stable kinetically and hardest one. The electrophilicity index (ω) were ranged from 8.45 to 23.52 eV, hence, all derivatives have strong electrophilicity character, as ω > 1.5 eV (Domingo et al., 2016, Afolabi et al., 2022), and may be sorted as **5b** < **5a** < **5c** < **7b** < **7c** < **7a** < **9c** < **9b** < **9a**. Alike, the electron donating

and acceptance powers data disclosed that their better proclivity to give electrons than getting where ω^+ values were less than ω^- (Domingo et al., 2016, Afolabi et al., 2022) (Table 1).

In consequence, the Mulliken's atomic charges, to give insight of intramolecular charge transfer and electronegativity (Bhagyasree et al., 2013), showed that the tetrazole nitrogen's has negative charges where the $N^1_{(tetz)}$ was lowest (-0.04) while $N^4_{(tetz)}$ was the highest (−0.16 - −0.18). In **5a-c**, both hydrazo atoms had a smaller negative charge than the thiazole nitrogen did ($NH_{(Hz)} = -0.16$, $N_{(Hz)} = -0.11$ and $N^3_{(thz)} =$ -0.24). Furthermore, the ketonic carbonyl oxygen were negatively charged in derivatives **7a-c** (−0.57) and **9a-c** (−0.43), the difference was attributed to the electron-release effect of thiophene ring is greater than the of thiadiazole. Also, the amino group nitrogen has higher negative charge than the phenylamino one ($NH_2 = -0.72$ and $NH_{(Pham)} = -0.48$) which may be assigned to involvement of the latter in the phenyl ring's resonance of. Finally, the sulfur atom in various heterocycles presented in all derivatives were positively charge (Table S4).

Furthermore, the electrophilic attack indices (f_k^-) of **5a-c** derivatives showed resemble order of susceptible atom in which the thiazolyl sulfur and carbon atoms ($S^1_{(thz)}$ and $C^5_{(thz)}$) occupied the top two positions, respectively. Likewise, the hybrids **7a-c** presented the thienyl sulfur atom ($S^1_{(thp)}$) occupied the first place followed by the thienyl carbon ($C^5_{(thp)}$) in **7a-b** while the amino nitrogen (NH_2) was located in the next pose in **7c**. However, the **9a-c** showed varied sequences, e.g., in **9a**, the phenyl carbon ($C^l_{(Phthdz)}$) inhabited the 1st position tailed with both cyano nitrogen atoms ($NC^1_{(MaNt)}$ and $NC^2_{(MaNt)}$), while in **9b**, the cyano nitrogen atom ($NC_{(CNAc)}$) appeared as the utmost dynamic position tailed with thiadiazolyl sulfur ($S^1_{(thdz)}$) and carbon ($C_{(CNAc)}$), respectively. On contrary, the relative electrophilicity descriptors (s_k^-/s_k^+) offered completely altered sorting than Fukui's indices. For instance, the hydrazo nitrogen ($NH_{(Hz)}$), thienyl carbon ($C^5_{(thp)}$) and phenylthiadiazole carbon ($C^2_{(Phthdz)}$) were the highly energetic sites in **5**, **7** and **9** derivatives, respectively (Table S5). Similarly, the Fukui's indices (f_k^+) suggested the thiazolyl sulfur atom ($S^1_{(thz)}$) and tetrazolyl nitrogen ($N^3_{(tetz)}$) were the most susceptible atoms in **5a-b** and **7a-b**, respectively. However, the phenyl carbon ($C^l_{(PhBenz)}$) in **5c** and the carbonyl oxygen (OC) in **7c** and **9a-c** were the most susceptible site, respectively. In contrary, the relative nucleophilicity descriptors (s_k^+/s_k^-) suggested varied fashions for the vulnerable atoms. Such as, the tetrazolyl nitrogen ($N^1_{(tetz)}$) was appeared on the top position in 5b and 7a-b whereas the phenyl tetrazolyl carbon ($C^2_{(Phtetz)}$) was the most active in derivatives **7c** and **9b-c** (Table S5).

The studied compounds have dipole moment (μ) ranged from 2.18 D, for **9c**, to 13.01 D, for **7b**, which greater than the urea's dipole as reference substance (Ahmed et al., 2008) by 1.58–9.47 times (Table 2). Also, the polarizability (α_{total}) data revealed that the **5a** and **9b** hybrids exhibited the smallest and biggest values, 2.43×10^{-23} and 3.28×10^{-23} esu, respectively. Nevertheless, the first-order hyperpolarizability data disclosed that the least and utmost value was found for the **9c** and **5b** derivatives, $\beta_{total} = 4.54 \times 10^{-30}$ and 1.09×10^{-29} esu, respectively. Accordingly, the investigated hybrids possessed higher hyperpolarizability than urea (Ahmed et al., 2008), 12.14–29.17 times, and may be sorted as **9c** < **9a** < **5c** < **9b** < **7a** < **7c** < **5a** < **7b** < **5b**.

4.3. Antimicrobial evaluation

Analogue **5a** displayed considerable antimicrobial activity against both *S. aureus* (10.37 μg/mL) and *S. pneumoniae* (12.78 μg/mL). Its efficacy against these bacteria suggests potential use in combatting Gram-positive infections, where ciprofloxacin reference displayed 4.82 and6.13 μg/mL in accordance to *S. aureus* and *S. pneumonia,* respectively. But against the Gram-negative bacteria, *S. typhimurium* and *E. coli*, **5a** had values of 16.22 and 9.93 μg/mL, respectively. Temporarily, ciprofloxacin reference displayed 2.53 and 4.62 μg/mL towards *S. typhimurium* and *E. coli,* respectively. The higher value against *S. typhimurium* indicates a lower potential efficacy in combatting this bacterium compared to *E. coli*. However, **5a** showed weak activity of 24.97 μg/mL against *C. albicans*, but there is no activity was appeared against *A. fumigatus*, which may suggest no activity. Meanwhile, **5b** showed good antimicrobial activity against *S. aureus* (7.29 μg/mL) and *S. pneumoniae* (9.61 μg/mL), quite consistent against both *S. typhimurium* (8.36 μg/mL) and *E. coli* (7.43 μg/mL), and had a high activity against *C. albicans* (28.26 μg/mL), yet there's no activity was recorded for *A. fumigatus*. However, miconazole reference displayed 27.60 and 25.29 μg/mL against *C. albicans* and *A. fumigatus*, respectively. In the meantime, analogue **5c** showed potent activity against *S. aureus* (6.61 μg/mL) and *S. pneumoniae* (7.92 μg/mL) compared to other analogues, had comparable values against *S. typhimurium* (7.11 μg/mL) and *E. coli* (6.33 μg/mL), and there's no activity appeared against *C. albicans*, **5c** demonstrated moderate reactivity against *A. fumigatus* (28.65 μg/mL) in contrast to reference (Miconazole) with 25.29 μg/mL. Moreover, analogue **7a** exhibited weak activity against *S. aureus* (10.16 μg/mL) and very weak against *S. pneumoniae* (14.37 μg/mL), For *S. typhimurium* and *E. coli*, it recorded values of 13.28 and 11.75 μg/mL, respectively, and good antifungal effectiveness against *C. albicans* (16.15 μg/mL), and respectable effectiveness against *A. fumigatus* (23.58 μg/mL). Whereas, analogue **7b** had proper antimicrobial values for *S. aureus* (7.62 μg/mL) and *S. pneumoniae* (9.83 μg/mL), showed acceptable activity values of 9.25 against *S. typhimurium* and 8.14 against *E. coli*, and there is no activity appeared against the examined fungal strainns. Even though, analogue **7c** displayed weak activity against *S. aureus* (8.74 μg/mL) and lower against *S. pneumoniae* (11.40 μg/mL), had values of 12.68 for *S. typhimurium* and 9.54 for *E. coli*, and demonstrated moderate effectiveness against *C. albicans* (29.38 μg/mL) and a good effectiveness against *A. fumigatus* (25.19 μg/mL). Furthermore, analogue **9a** showed the lowest activity against *S. aureus* (14.63 μg/mL) and *S. pneumoniae* (17.49 μg/mL) among the rest derivatives. Surprisingly, had the potent efficacy against both *S. typhimurium* (4.27 μg/mL), and E. *coli* (5.28 μg/mL) with a weak effective against both fungi, *C. albicans* (31.19 μg/mL) and *A. fumigatus* (29.32 μg/mL). In the meantime, analogue **9b** exhibited weak activity against *S. aureus* (11.44 μg/mL) and *S. pneumoniae* (13.29 μg/mL), demonstrated a moderate activity against *S. typhimurium* (6.35 μg/mL) and *E. coli* (6.19 μg/mL), and had significant activity against *C. albicans* (21.27 μg/mL), no activity was appeared for *A. fumigatus*. Besides, analogue **9c** represented values of 13.21 μg/mL against *S. aureus* and 12.43 μg/mL against *S. pneumoniae*, relatively consistent activity with values of 5.29 for *S. typhimurium* and 7.30 μg/mL for *E. coli*, and there is no activity recorded against fungi. The data suggests that the antimicrobial activities of the analogues vary widely against different microbes. Analogue **9a** consistently demonstrated significant antimicrobial activity against Gram (−ve) bacteria.

4.4. Structure activity relationship (SAR)

Inspired the chemical structures of the synthesized tetrazole hybridized with thiazole, thiophene or thiadiazole derivatives their antimicrobial reactivity relationship showed interested facts. The presence of a *p*-tolyl group in analogue **5a** might contribute to its broad-spectrum activity. Where a methyl substituent often enhance lipophilicity, potentially aiding in cell penetration (Silverman and Holladay, 2014). While analogue **5b** with *p*-methoxyphenyl group, being electron-donating, can influence the reactivity of aromatic rings. The enhanced antifungal activity could be attributed to potential interactions of the methoxy group with fungal enzyme systems or cellular components (Eicher et al., 2013). Though, analogue **5c** with *p*-chlorophenyl moiety: Halogens like chlorine can partake in bonding with biomolecules. From the previous literature and the results of the antibacterial effectiveness according to the MIC values in Table 3, it could be concluded that the order of reactivity of the synthesized analogues **5a-c** was arranged as follows: **5c** > **5b** > **5a**. The specificity towards *A. fumigatus* might be due to specific interactions the chlorine has with proteins or enzymes present

predominantly in this fungus (Metrangolo and Resnati, 2008). On the other hand, tetrazole linked thiophene derivatives: analogue **7a** with 3-amino, 4-Cyano thiophene: Amino groups can form hydrogen bonds, while cyano groups can act as electron-withdrawing groups, increasing the electrophilicity of the molecule. This dual presence might enhance its interaction with bacterial and fungal targets (Shaker et al., 2021). Meanwhile, analogue **7b** with 3-amino, 4-Carboethoxy thiophene: Carboethoxy groups introduce ester functionalities. Ester groups might decrease antimicrobial properties due to potential hydrolysis or metabolism in microbial systems (Leeson and Springthorpe, 2007). Temporarily, analogue **7c** have 3-amino, 4-Carboamido thiophene: Carboamido groups can partake in multiple hydrogen bonding, which can increase specificity and affinity to microbial targets, explaining its potency against *C. albicans* (Bissantz et al., 2010). Based on the prior literature and the findings of antibacterial efficiency based on MIC values in Table 3, it was possible to determine that the sequence of reactivity of the synthesized analogues **7a-c** was as follows: **7b** > **7c** > **7a**. Moreover, insight the tetrazole linked thiadiazole derivatives: analogue **9a** with dicyano-thiazdiazole: Dicyano groups can significantly increase the molecule's polarity. The enhanced activity against Gram-positive bacteria might be due to better penetration through the thick peptidoglycan layer (Lambert, 2002).Whoever, analogue **9b** with cyano and carboethoxy thiadiazole: The combined presence of cyano and carboethoxy groups might provide a weak effect the two diverse electron-withdrawing groups rather than the effect of two nitrile groups in hybrid **9a**, impacting its antimicrobial profile. Furthermore, analogue **9c** with cyano and carbamido thiadiazole: The carbamido group's hydrogen bonding potential, combined with the electron-withdrawing nature of the cyano group, might guide its activity mainly towards Gram-positive bacteria. In Conclusion, the antimicrobial activities of the synthesized tetrazole hybridized with thiazole, thiophene or thiadiazole derivatives showcase the pivotal role of functional groups in dictating specificity and potency.

4.5. Molecular docking

Insight the molecular docking, hybrid **5a** showed diverse interactions involving H-bond donors and acceptors and Pi-H interactions, prominently with Thr 194, Gln 197, and His 46 (Figure S3). The interaction distances were within 2.95 to 3.89 Å, signifying close and possibly strong interactions. Meanwhile, hybrid **5b** primarily interacted with Arg 200 *via* N12 of the tetrazole ring, acting as a H-bond acceptor (Fig. 5). In the meantime, hybrid **5c** showed a Pi-H interaction between its thiazole ring and Pro 87 (Figure S3).

Moreover, hybrid **7a** exhibited a H-bond acceptor interaction involving its carbonyl group with Arg 144. While hybrid **7b** presented a Pi-H interaction between its phenyl ring and Ile 86. Whereas hybrid **7c** showcased a Pi-H interaction of its tetrazole-ring with Ile 175 (Figure S4). Furthermore, hybrid **9a** demonstrated a spectrum of interactions with various amino acids of PDB: 4URO. Notably, it established multiple hydrogen bond interactions, including those with Ser 128, Arg 144, Gly 83, and Gly 85. It also showed Pi-H interactions with Pro 87 and Arg 200 (Fig. 6). Besides, hybrid **9b** formed H-bond interactions with Gly 85 and Arg 144, with the ligand's thiadiazole ring and nitrile group being the donors and acceptors, respectively (Figure S6). Also, hybrid **9c** too had an array of interactions, including H-bonds with Ser 128, Gly 83, and Gly 85. A Pi-H interaction was also noticed with Pro 87 (Fig. 6).

On the other hand, Spiro reference exhibited the highest RMSD = 1.3823 through binding affinity = −6.7132 kcal/mol, interacted with Asp 81 *via* the C 2 of the pyridone ring, serving as a H-bond donor (Figure S6). Finally, our findings reveal each ligand's precise interaction profile, giving a structural basis for their binding affinities. Understanding such interactions is critical in drug development procedures since it aids in rationalising biological activity and lays the groundwork for subsequent chemical optimisation. Specific functional groups in the ligands clearly play important roles in mediating interactions with target residues, which can lead subsequent structural alterations for increased activity.

The tetrazole hybridized with thiazole, thiophene, or thiadiazole derivatives found in all of the synthesised analogues, on the other hand, made it simpler for them to create H-bonds and Pi-H interactions with 4URO amino acids. According to three-dimensional images, the most pockets of 4URO, consisting of Arg 200, Arg 144, Gly 83, Gly 85, and Pro 87, provided an appropriate hole for the produced tetrazole hybridized with thiazole, thiophene, or thiadiazole derivatives. Several amino-acids were widely speared onto the protein shallow throughout the mapping of numerous diverging from the reference conformations to locate consensus regions. Three-dimensional images probes have been duplicated by employing docking simulation to build new crystal structure conformations.

5. Conclusion

The design and synthesis of nine hybrids containing tetrazole core and thiazole, thiophene or thiadiazole ring systems were described. The synthetic strategy is based on the reactions of 1-(4-(2-bromoacetyl)-phenyl)-1*H*-tetrazole with thiosemicarbazone derivatives **4a-c** for the production of tetrazole-thiazole hybrids **5a-c**, while the reaction with thiocarbamoyl derivatives **6a-c** was the route for the tetrazole-thiophene hybrids **7a-c**. The chemical behavior reaction of 2-(4-(1*H*-tetrazol-1-yl)phenyl)-*N*-(4-chlorophenyl)-2-oxoacetohydrazonoyl

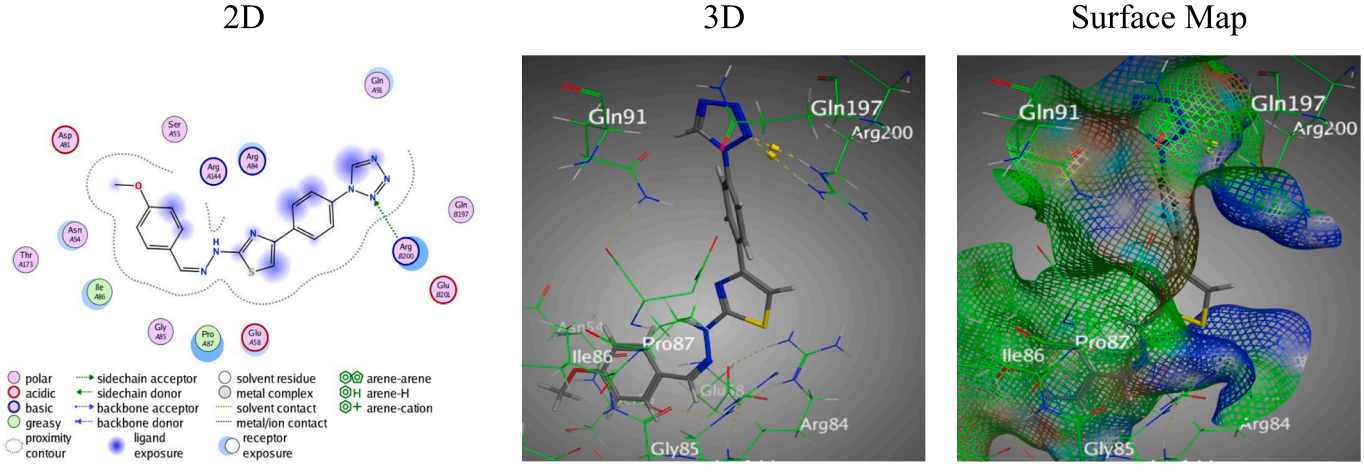

Fig. 5. Docking results of hybrid **5b** with PDB: 4URO.

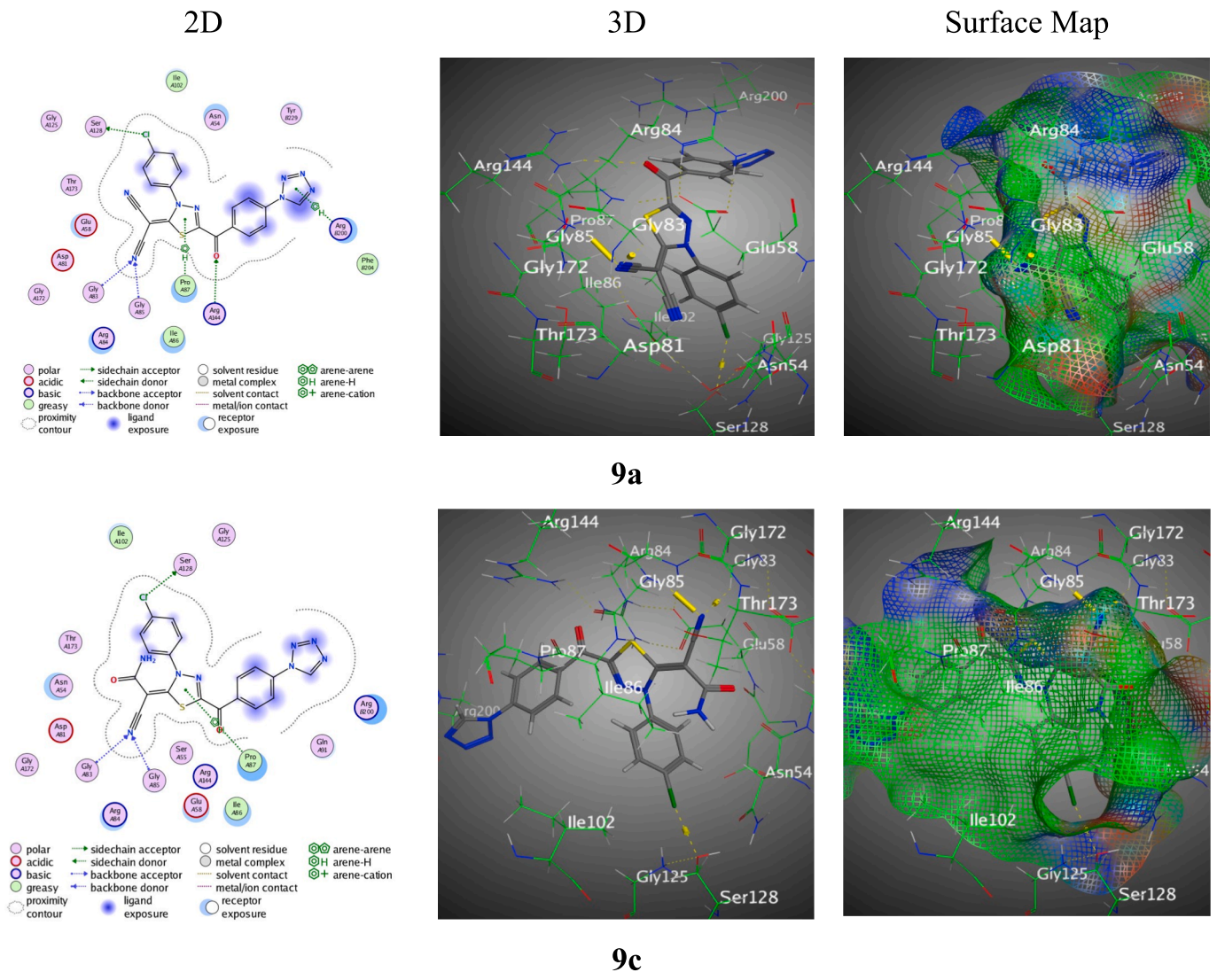

Fig. 6. Docking results of hybrids **9a** and **9c** with PDB: 4URO.

bromide (**8**) towards the thiocarbamoyl compounds **6a-c** allowed for separation of tetrazole-thiadiazole hybrids **9a-c**. The thiadiazole derivatives **9a-c** exhibited the lower HOMO-LUMO energies than thiophenes **7a-c** and thiazoles **5a-c**, respectively, and may be arranged as **9a** < **9b** < **9c** < **7a** < **7c** < **7b** < **5a** = **5b** = **5c**. Also, the first-order hyperpolarizability data, on comparison with the urea's, indicated that all studied compounds possessed higher hyperpolarizability than urea, 12.14–29.17 times. The antibacterial efficacy of tetrazole derivatives against bacterial and fungal strains showed that the synthesized tetrazole-hybrids **5b**, **5c**, and **7b** shown good antibacterial action against two +ve gram bacterial strains (*S. aureus* and *S. pneumonia*), whereas the synthesized tetrazole-hybrids **9a-c** had strong activity against two −ve gram bacterial strains (*S. typhimurium* and *E. coli*). Meanwhile, tetrazole-hybrids **5a**, **7a** and **9b** demonstrated robust efficacy against fungal strain (*C. albicans*), tetrazole-hybrids **7a** and **7c** demonstrated good efficacy against (A. *fumigatus*). Furthermore, tetrazole compounds coupled with thiazole, thiophene, or thiadiazole were stimulated to assess their binding relationship against PDB ID: 4URO, hybrids **9a**, **9b**, and **7c** revealed strong binding interactions through several H-donor, H-acceptor, and Pi-H bonds.

Declaration of competing interest

The authors declare that they have no known competing financial interests or personal relationships that could have appeared to influence the work reported in this paper.

Appendix A. Supplementary material

Supplementary data to this article can be found online at https://doi.org/10.1016/j.jsps.2024.101962.

References

Abraham, J.P., Sajan, D., Joe, I.H., Jayakumar, V.S., 2008. Molecular structure, spectroscopic studies and first-order molecular hyperpolarizabilities of p-amino acetanilide. Spectrochim. Acta Part a, Mol. Biomol. Spectros. 71 (2), 355–367.

Afolabi, S.O., Semire, B., Akiode, O.K., et al., 2022. Quantum study on the optoelectronic properties and chemical reactivity of phenoxazine-based organic photosensitizer for solar cell purposes. Theo. Chem. Acc. 141, 1–14.

Ahmadi, A., Mohammadnejadi, E., Karami, P., Razzaghi-Asl, N., 2022. Current status and structure activity relationship of privileged azoles as antifungal agents (2016–2020). Int. J. Antimicrob. Agents 59 (3), 106518.

Ahmed, A.B., Feki, H., Abid, Y., Boughzala, H., Mlayah, A., 2008. Structural, vibrational and theoretical studies of l-histidine bromide. J. Mol. Struct. 888 (1-3), 180–186.

Arshad, M.F., Alam, A., Alshammari, A.A., Alhazza, M.B., Alzimam, I.M., Alam, M.A., Mustafa, G., Ansari, M.S., Alotaibi, A.M., Alotaibi, A.A., Kumar, S., Asdaq, S.M.B., Imran, M., Deb, P.K., Venugopala, K.N., Jomah, S., 2022. Thiazole: A versatile standalone moiety contributing to the development of various drugs and biologically active agents. Molecules 27 (13), 3994.

Aziz, M., Ejaz, S.A., Tamam, N., Siddique, F., Riaz, N., Qais, F.A., Chtita, S., Iqbal, J., 2022. Identification of potent inhibitors of NEK7 protein using a comprehensive

computational approach. Sci Rep. 12 (1) https://doi.org/10.1038/s41598-022-10253-5.
Baranwal, J., Kushwaha, S., Singh, S., Jyoti, A., 2023. A Review on the Synthesis and Pharmacological Activity of Heterocyclic Compounds. Curr. Phys. Chem. 13 (1), 2–19.
Becke, A. D., 1993. Density-functional thermochemistry. III. The role of exact exchange. J. Chem. Phys. 98, 5648-5652.
Beno, B.R., Yeung, K.-S., Bartberger, M.D., Pennington, L.D., Meanwell, N.A., 2015. A Survey of the Role of Noncovalent Sulfur Interactions in Drug Design. J Med Chem. 58 (11), 4383–4438.
Bhagyasree, J.B., Varghese, H.T., Panicker, C.Y., Samuel, J., Van Alsenoy, C., Bolelli, K., Yildiz, I., Aki, E., 2013. Vibrational spectroscopic (FT-IR, FT-Raman, (1)H NMR and UV) investigations and computational study of 5-nitro-2-(4-nitrobenzyl) benzoxazole. Spectrochim. Acta Part a, Mol. Biomol. Spectros. 102, 99–113.
Biovia, D.S., 2017. Materials Studio. Dassault Systèmes, San Diego.
Bissantz, C., Kuhn, B., Stahl, M., 2010. A medicinal chemist`s guide to molecular interactions. J. Med. Chem. 53 (14), 5061–5084.
Bouchoucha, A., Zaater, S., Bouacida, S., Merazig, H., Djabbar, S., 2018. Synthesis and characterization of new complexes of nickel (II), palladium (II) and platinum(II) with derived sulfonamide ligand: Structure, DFT study, antibacterial and cytotoxicity activities. J. Mol. Struct. 1161, 345–355.
Bredael, K., Geurs, S., Clarisse, D., De Bosscher, K., D'hooghe, M., Trabocchi, A., 2022. Carboxylic acid bioisosteres in medicinal chemistry: synthesis and properties. J. Chem. 2022, 1–21.
Bulat, F.A., Chamorro, E., Fuentealba, P., Toro-Labbé, A., 2004. Condensation of frontier molecular orbital Fukui functions. J. Phys. Chem. a. 108 (2), 342–349.
Cardoso-Ortiz, J., Leyva-Ramos, S., Baines, K.M., Gómez-Durán, C.F.A., Hernández-López, H., Palacios-Can, F.J., Valcarcel-Gamiño, J.A., Leyva-Peralta, M.A., Razo-Hernández, R.S., 2023. Novel ciprofloxacin and norfloxacin-tetrazole hybrids as potential antibacterial and antiviral agents: Targeting S. aureus topoisomerase and SARS-CoV-2-MPro. J. Mol. Struct. 1274, 134507.
Delley, B., 2006. Ground-state enthalpies: evaluation of electronic structure approaches with emphasis on the density functional method. J. Phys. Chem. a. 110, 13632–13639. https://doi.org/10.1021/jp0653611.
Dennington, R., Keith, T., Millam, J., 2009. GaussView, version 5. Semichem Inc., Shawnee Mission, KS.
Domingo, L.R., Rios-Gutierrez, M., Perez, P., 2016. Applications of the Conceptual Density Functional Theory Indices to Organic Chemistry Reactivity. Molecules 21, 748. https://doi.org/10.3390/molecules21060748.
Eicher, T., Hauptmann, S., Speicher, A., 2013. The chemistry of heterocycles: structures, reactions, synthesis, and applications. John Wiley & Sons.
El Adnani, Z., Mcharfi, M., Sfaira, M., Benzakour, M., Benjelloun, A.T., Ebn Touhami, M., 2013. DFT theoretical study of 7-R-3methylquinoxalin-2 (1H)-thiones (RH; CH3; Cl) as corrosion inhibitors in hydrochloric acid. Corros. Sci. 68, 223–230.
Fathallah, N., Raafat, M.M., Issa, M.Y., Abdel-Aziz, M.M., Bishr, M., Abdelkawy, M.A., Salama, O., 2019. Bio-guided fractionation of prenylated benzaldehyde derivatives as potent antimicrobial and antibiofilm from Ammi majus L. fruits-associated Aspergillus amstelodami. Molecules 24 (22), 4118.
Frisch, M., G. Trucks, H. Schlegel, et al., 2009. Gaussian 09W. Wallingford, CT, USA, Gaussian. Inc.
Gehringer, M., Laufer, S.A., 2019. Emerging and re-emerging warheads for targeted covalent inhibitors: applications in medicinal chemistry and chemical biology. J. Med. Chem. 62 (12), 5673–5724.
Gomha, S.M., Kheder, N.A., Abdelaziz, M.R., Mabkhot, Y.N., Alhajoj, A.M., 2017. A facile synthesis and anticancer activity of some novel thiazoles carrying 1,3,4-thiadiazole moiety. Chem. Cent. J. 11, 25.
Hoque, J., Sangaj, N., Varghese, S., 2019. Stimuli-responsive supramolecular hydrogels and their applications in regenerative medicine. Macromol. Biosci. 19, 1800259.
Jain, A.K., Sharma, S., Vaidya, A., Ravichandran, V., Agrawal, R.K., 2013. 1,3,4-thiadiazole and its derivatives: a review on recent progress in biological activities. Chem Biol Drug Des. 81 (5), 557–576.
Karamanis, P., Pouchan, C., Maroulis, G., 2008. Structure, stability, dipole polarizability and differential polarizability in small gallium arsenide clusters from all-electron ab initio and density-functional-theory calculations. Phys. Rev. A: At. Mol. Opt. Phys. 77, 013201.
Khan, M.U., Khalid, M., Shafiq, I., Khera, R.A., Shafiq, Z., Jawaria, R., Shafiq, M., Alam, M.M., Braga, A.A.C., Imran, M., Kanwal, F., Xu, Z., Lu, C., 2021. Theoretical investigation of nonlinear optical behavior for rod and T-Shaped phenothiazine based D-π-A organic compounds and their derivatives. J. Saudi Chem. Soc. 25 (10), 101339.
Kotian, S.Y., Mohan, C.D., Merlo, A.A., Rangappa, S., Nayak, S.C., Rai, K.M.L., Rangappa, K.S., 2020. Small molecule based five-membered heterocycles: A view of liquid crystalline properties beyond the biological applications. J. Mol. Liq. 297, 111686.
Lambert, P., 2002. Cellular impermeability and uptake of biocides and antibiotics in Gram-positive bacteria and mycobacteria. J. Appl. Microbiol. 92, 46S–54S.
Lee, C., Yang, W., Parr, R.G., 1988. Development of the Colle-Salvetti correlation-energy formula into a functional of the electron density. Phys. Rev. b: Condens. Matter. 37 (2), 785–789.
Leeson, P.D., Springthorpe, B., 2007. The influence of drug-like concepts on decision-making in medicinal chemistry. Nat. Rev. Drug Discov. 6, 881–890. https://doi.org/10.1038/nrd2445.
Levin, J. I., 1997. The development of nonpeptide angiotensin II-receptor antagonists.
Liu, J.-C., Narva, S., Zhou, K., Zhang, W., 2019a. A review on the antitumor activity of various nitrogenous-based heterocyclic compounds as NSCLC inhibitors. Mini-Rev. Med. Chem. 19 (18), 1517–1530.
Liu, J., Ren, Z., Fan, L.i., Wei, J., Tang, X., Xu, X., Yang, D., 2019b. Design, synthesis, biological evaluation, structure-activity relationship, and toxicity of clinafloxacin-azole conjugates as novel antitubercular agents. Bioorg. Med. Chem. 27 (1), 175–187.
Makhlouf, M.M., Radwan, A.S., Ghazal, B., 2018. Experimental and DFT insights into molecular structure and optical properties of new chalcones as promising photosensitizers towards solar cell applications. Appl. Surf. Sci. 452, 337–351.
Marsh, R.E., 2004. Space group Cc: an update. Acta Crystallogr b. 60, 252–253. https://doi.org/10.1107/S0108768104003878.
Mermer, A., Bayrak, H., Şirin, Y., Emirik, M., Demirbaş, N., 2019. Synthesis of novel Azol-β-lactam derivatives starting from phenyl piperazine and investigation of their antiurease activity and antioxidant capacity comparing with their molecular docking studies. J. Mol. Struct. 1189, 279–287.
Messali, M., Larouj, M., Lgaz, H., Rezki, N., Al-Blewi, F.F., Aouad, M.R., Chaouiki, A., Salghi, R., Chung, I.-M., 2018. A new schiff base derivative as an effective corrosion inhibitor for mild steel in acidic media: Experimental and computer simulations studies. J. Mol. Struct. 1168, 39–48.
Metrangolo, P., Resnati, G. (Eds.), 2008. Structure and BondingHalogen Bonding. Springer Berlin Heidelberg, Berlin, Heidelberg.
Mi, H., Xiao, G., Chen, X., 2015. Theoretical evaluation of corrosion inhibition performance of three antipyrine compounds. Comput. Theor. Chem. 1072, 7–14.
Oballa, R.M., Belair, L., Black, W.C., Bleasby, K., Chan, C.C., Desroches, C., Du, X., Gordon, R., Guay, J., Guiral, S., Hafey, M.J., Hamelin, E., Huang, Z., Kennedy, B., Lachance, N., Landry, F., Li, C.S., Mancini, J., Normandin, D., Pocai, A., Powell, D.A., Ramtohul, Y.K., Skorey, K., Sørensen, D., Sturkenboom, W., Styhler, A., Waddleton, D.M., Wang, H., Wong, S., Xu, L., Zhang, L., 2011. Development of a liver-targeted stearoyl-CoA desaturase (SCD) inhibitor (MK-8245) to establish a therapeutic window for the treatment of diabetes and dyslipidemia. J Med Chem. 54 (14), 5082–5096.
Olasunkanmi, L.O., Obot, I.B., Ebenso, E.E., 2016. Adsorption and corrosion inhibition properties of N-{n-[1-R-5-(quinoxalin-6-yl)-4, 5-dihydropyrazol-3-yl] phenyl} methanesulfonamides on mild steel in 1 M HCl: experimental and theoretical studies. RSC Adv. 6 (90), 86782–86797.
Omar, M.A., Masaret, G.S., Abbas, E.M.H., Abdel-Aziz, M.M., Harras, M.F., Farghaly, T. A., 2020. Novel anti-tubercular and antibacterial based benzosuberone-thiazole moieties: Synthesis, molecular docking analysis, DNA gyrase supercoiling and ATPase activity. Bioorg Chem. 104, 104316.
Peerzada, M.N., Hamel, E., Bai, R., Supuran, C.T., Azam, A., 2021. Deciphering the key heterocyclic scaffolds in targeting microtubules, kinases and carbonic anhydrases for cancer drug development. Pharmacol. Ther. 225, 107860.
Perdew, J.P., Wang, Y., 1992. Pair-distribution function and its coupling-constant average for the spin-polarized electron gas. Phys Rev B Condens Matter. 46, 12947–12954. https://doi.org/10.1103/physrevb.46.12947.
Petrou, A., Fesatidou, M., Geronikaki, A., 2021. Thiazole ring—A biologically active scaffold. Molecules 26, 3166.
Prasad, P.N., Williams, D.J., 1991. Introduction to nonlinear optical effects in molecules and polymers. Wiley, New York.
Preetham, R., Vijaya Kumar, M.S., Swaroop, T.R., Divyashree, S., Kiran, K.R., Sreenivasa, M.Y., Sadashiva, M.P., Rangappa, K.S., 2022. An Efficient Route for the Synthesis of 1, 5-Disubstituted Tetrazoles and their Anti-Microbial Activity Against Salmonella Paratyphi. ChemistrySelect 7 (45).
Roszkowski, P., Szymańska-Majchrzak, J., Koliński, M., Kmiecik, S., Wrzosek, M., Struga, M., Szulczyk, D., 2021. Novel Tetrazole-Based Antimicrobial Agents Targeting Clinical Bacteria Strains: Exploring the Inhibition of Staphylococcus aureus DNA Topoisomerase IV and Gyrase. Int J Mol Sci. 23 (1), 378.
Roy, R.K., de Proft, F., Geerlings, P., 1998a. Site of protonation in aniline and substituted anilines in the gas phase: a study via the local hard and soft acids and bases concept. J. Phys. Chem. a. 102 (35), 7035–7040.
Roy, R. K., S. Pal and K. Hirao, 1999. On non-negativity of Fukui function indices. J. Chem. Phys. 110, 8236-8245.
Roy, R.K., Krishnamurti, S., Geerlings, P., Pal, S., 1998b. Local softness and hardness based reactivity descriptors for predicting intra-and intermolecular reactivity sequences: carbonyl compounds. J. Phys. Chem. a. 102 (21), 3746–3755.
Sajan, D., Joseph, L., Vijayan, N., Karabacak, M., 2011. Natural bond orbital analysis, electronic structure, non-linear properties and vibrational spectral analysis of L-histidinium bromide monohydrate: a density functional theory. Spectrochim. Acta A Mol. Biomol. Spectrosc. 81 (1), 85–98.
Serban, G., Stanasel, O., Serban, E., et al., 2018. 2-Amino-1, 3, 4-thiadiazole as a potential scaffold for promising antimicrobial agents. Drug Des. Devel. Ther. 1545–1566.
Shaker, B., Ahmad, S., Lee, J., Jung, C., Na, D., 2021. In silico methods and tools for drug discovery. Comput. Biol. Med. 137, 104851.
Shi, Y., 2001. Particle swarm optimization: developments, applications and resources. Proceedings of the 2001 congress on evolutionary computation, IEEE Cat. No. 01TH8546.
Shukla, P.K., Verma, A., Mishra, P., 2017. Significance of nitrogen heterocyclic nuclei in the search of pharmacological active compounds. New Perspect. Agric. Human Health 100–126.
Silverman, R.B., Holladay, M.W., 2014. The organic chemistry of drug design and drug action. Academic press.
Studzińska, R., Karczmarska-Wódzka, A., Kozakiewicz, A., Kołodziejska, R., Paprocka, R., Wróblewski, M., Augustyńska, B., Modzelewska-Banachiewicz, B., 2015. 2-Allylaminothiazole and 2-allylaminodihydrothiazole derivatives: synthesis, characterization, and evaluation of bioactivity. Monatsh. Chem. 146 (10), 1673–1679.

Sun, Y., Chen, X., Sun, L., Guo, X., Lu, W., 2003. Nanoring structure and optical properties of Ga8As8. Chem. Phys. Lett. 381 (3-4), 397–403.
Tunney, M.M., Ramage, G., Field, T.R., Moriarty, T.F., Storey, D.G., 2004. Rapid colorimetric assay for antimicrobial susceptibility testing of Pseudomonas aeruginosa. Antimicrob. Agents Chemother. 48 (5), 1879–1881.
Vembu, S., Pazhamalai, S., Gopalakrishnan, M., 2016. Synthesis, spectral characterization, and effective antifungal evaluation of 1H-tetrazole containing 1, 3, 5-triazine dendrimers. Med. Chem. Res. 25 (9), 1916–1924.
Williams, D.J., 1984. Organic polymeric and non-polymeric materials with large optical nonlinearities. Angew. Chem. Int. Ed. 23 (9), 690–703.
Wu, Y.-J., Meanwell, N.A., 2021. Geminal diheteroatomic motifs: some applications of acetals, ketals, and their sulfur and nitrogen homologues in medicinal chemistry and drug design. J. Med. Chem. 64 (14), 9786–9874.
Xavier, S., Periandy, S., Ramalingam, S., 2015. NBO, conformational, NLO, HOMO–LUMO, NMR and electronic spectral study on 1-phenyl-1-propanol by quantum computational methods. Spectrochim. Acta A Mol. Biomol. Spectrosc. 137, 306–320. https://doi.org/10.1016/j.saa.2014.08.039.

Further reading

Hsiao, W.-W., Le, T.-N., Pham, D.M., Ko, H.-H., Chang, H.-C., Lee, C.-C., Sharma, N., Lee, C.-K., Chiang, W.-H., 2021. Recent Advances in Novel Lateral Flow Technologies for Detection of COVID-19. Biosensors 11 (9), 295.